Global frequency and distribution of lightning as observed from space by the Optical Transient Detector

Hugh J. Christian,[1] Richard J. Blakeslee,[1] Dennis J. Boccippio,[1] William L. Boeck,[2] Dennis E. Buechler,[3] Kevin T. Driscoll,[3] Steven J. Goodman,[1] John M. Hall,[4] William J. Koshak,[1] Douglas M. Mach,[3] and Michael F. Stewart[3]

Received 20 March 2002; revised 18 June 2002; accepted 23 June 2002; published 3 January 2003.

[1] The Optical Transient Detector (OTD) is a space-based instrument specifically designed to detect and locate lightning discharges as it orbits the Earth. This instrument is a scientific payload on the MicroLab-1 satellite that was launched into a 70° inclination low Earth orbit in April 1995. Given the orbital trajectory of the satellite, most regions of the Earth are observed by the OTD instrument more than 400 times during a 1 year period, and the average duration of each observation is 2 min. The OTD instrument optically detects lightning flashes that occur within its 1300 × 1300 km^2 field of view during both day and night conditions. A statistical examination of OTD lightning data reveals that nearly 1.4 billion flashes occur annually over the entire Earth. This annual flash count translates to an average of 44 ± 5 lightning flashes (intracloud and cloud-to-ground combined) occurring around the globe every second, which is well below the traditional estimate of 100 fl s^{-1} that was derived in 1925 from world thunder day records. The range of uncertainty for the OTD global totals represents primarily the uncertainty (and variability) in the flash detection efficiency of the instrument. The OTD measurements have been used to construct lightning climatology maps that demonstrate the geographical and seasonal distribution of lightning activity for the globe. An analysis of this annual lightning distribution confirms that lightning occurs mainly over land areas, with an average land/ocean ratio of ~10:1. The Congo basin, which stands out year-round, shows a peak mean annual flash density of 80 fl km^{-2} yr^{-1} in Rwanda, and includes an area of over 3 million km^2 exhibiting flash densities greater than 30 fl km^{-2} yr^{-1} (the flash density of central Florida). Lightning is predominant in the northern Atlantic and western Pacific Ocean basins year-round where instability is produced from cold air passing over warm ocean water. Lightning is less frequent in the eastern tropical Pacific and Indian Ocean basins where the air mass is warmer. A dominant Northern Hemisphere summer peak occurs in the annual cycle, and evidence is found for a tropically driven semiannual cycle. *INDEX TERMS:* 3304 Meteorology and Atmospheric Dynamics: Atmospheric electricity; 3309 Meteorology and Atmospheric Dynamics: Climatology (1620); 3324 Meteorology and Atmospheric Dynamics: Lightning; 3394 Meteorology and Atmospheric Dynamics: Instruments and techniques; *KEYWORDS:* lightning, thunderstorm, atmospheric electricity, convection, climatology, remote sensing

Citation: Christian, H. J., et al., Global frequency and distribution of lightning as observed from space by the Optical Transient Detector, *J. Geophys. Res.*, *108*(D1), 4005, doi:10.1029/2002JD002347, 2003.

1. Introduction

[2] Recent interest in how global lightning activity might change in the future as a result of global warming [*Williams*, 1992], and how the distribution and frequency of lightning activity changes from year to year as a result of the El Niño–Southern Oscillation (ENSO) phenomena [*Goodman and Christian*, 1993; *Goodman et al.*, 2000; *Hamid et al.*, 2001], has led to renewed interest in determining the global flash rate. The global chemical transport models used to understand the impacts of trace gases and the variations in the Earth's ozone are requiring increased spatial and temporal details of global lightning, an important natural source of NO_x. Lightning frequency is used in the parameterization and validation of such models [e.g., *Levy et al.*, 1996].

[3] Prior studies have attempted to estimate the global flash rate and determine the contribution of thunderstorm activity to the maintenance of the global electric circuit [*Brooks*, 1925; *Williams and Heckman*, 1993]. *Brooks* [1925] estimated that the Earth has 1800 thunderstorms

[1]NASA Marshall Space Flight Center, Huntsville, Alabama, USA.
[2]Niagara University, Niagara, New York, USA.
[3]University of Alabama in Huntsville (UAH), Huntsville, Alabama, USA.
[4]CSC Huntsville, Huntsville, Alabama, USA.

0148-0227/03/2002JD002347$09.00

occurring at any instant around the world each producing 200 fl h^{-1} on average (or 3.3 fl min^{-1}; comparable to a mean satellite-observed thunderstorm cell flash rate of 3.1 fl min^{-1} [*Williams et al.*, 2000, after applying calibrations described in this paper]). From this, Brooks inferred that the average global flash rate is 100 fl s^{-1}. Since the advent of satellite technology, several spaceborne instruments have measured the global distribution of lightning either as a primary research objective or an unanticipated bonus (see *Goodman and Christian* [1993] for a review of prior observations). *Kotaki and Katoh* [1983] estimated a global average flash rate of 63 fl s^{-1} using radio frequency receivers on the ISS-b satellite during the period June 1978 to May 1980. *Mackerras et al.* [1998] estimated a global average flash rate of 65 fl s^{-1} through an intercomparison of ground-based observations at selected locations around the world with the ISS-b measurements and Defense Meteorological Satellite Program (DMSP) nighttime lightning observations [*Orville and Henderson*, 1986; *Goodman and Christian*, 1993]. The uncertainty in these estimates was stated to be a factor of two. More recently, *Heckman et al.* [1998] used Schumann resonance (SR) observations to infer constraints on either the global flash rate or average dipole moment changes of flashes. Using a small sample of actual moment change observations, they found that a global flash rate of 22 fl s^{-1} could be consistent with the SR observations.

[4] Much of the prior research was hampered by the absence of measurements that accurately quantify the frequency and distribution of lightning activity for the Earth. The problems included: low or unknown detection efficiency, poor spatial and temporal resolution, a limited number or brief periods of observations, and incomplete sampling of the diurnal cycle. As a result of these deficiencies, the thunder day statistics determined by human observers and compiled by the *World Meteorological Organization* (*WMO*) [1953] is one of the best sources of proxy information concerning lightning activity worldwide.

[5] The Optical Transient Detector (OTD) is one of the latest space-based instruments specifically designed to detect lightning worldwide. It is a scientific payload on the MicroLab-1 satellite (renamed OV-1), which was launched into low Earth orbit on 3 April 1995. The geolocated data used in the OTD climatology presented here span the period 4 May 1995 to 21 March 2000. By compositing 5 years of OTD lightning data, it is possible to determine the average number of flashes that occur over the course of a year and their spatial distribution. The scope of this study is the presentation and analysis of the average annual and seasonal worldwide distribution of total lightning activity. Key aspects of the climatology are discussed, including global extrema, regional differences, land/ocean variability, and zonal and meridional decomposition. Variability on other timescales, including diurnal and interannual, will be addressed in future studies.

2. Methodology

2.1. Instrument Description and Characteristics

[6] The OTD instrument consists of a staring imager optimized to detect and locate lightning during the day and night. An imaging system, a focal plane assembly, real-time event processor, a formatter, power supply, and interface electronics are the major subsystems of the sensor. The entire instrument, which is divided into a sensor assembly and the electronics unit, weighs approximately 20 kg, consumes less than 25 W of power, and requires a telemetry data rate of only 6 kb s^{-1}.

[7] The sensor assembly consists of a wide field-of-view telescope, a narrow band interference filter, and a high speed mosaic array focal plane. The imaging system is a fast f/1.6 telescope with a 3.3 mm aperture that provides a $75° \times 75°$ full-angle field of view with a maximum angle of 5° at the interference filter. The focal plane assembly and drive electronics includes a 128×128 element charge coupled device (CCD), a clock, preamplifiers, and multiplexers, which permit an imaging rate of 500 frames per second. The interference filter has a narrow bandwidth (0.856 nm at half-maximum) [*Koshak et al.*, 2000a] and is centered on the OI(1) neutral atomic oxygen multiplet at 777.4 nm [*Orville and Henderson*, 1984].

[8] The specific characteristics of the sensor design result from the requirement to detect weak lightning signals during the day when the background illumination produced by sunlight reflecting from the tops of clouds is much brighter than the illumination produced by lightning. Consequently, the daytime lightning signals tend to be buried in the background noise, and the only way to detect lightning during daytime is to implement techniques that increase or maximize the lightning signal relative to this bright background. The OTD design takes advantage of the significant differences in the temporal, spatial, and spectral characteristics between the lightning signal and the background noise [*Christian et al.*, 1989].

[9] A combination of four methods are employed by the OTD for optimizing the signal-to-noise ratio. First, spatial filtering is used which matches the instantaneous field of view of each detector element in the OTD focal plane array (CCD pixel) to a typical cloud top area illuminated by a lightning stroke (i.e., ~10 km). This results in an optimized sampling of the lightning scene relative to the background illumination while reducing the likelihood of splitting the signal between adjacent CCD pixels [*Christian et al.*, 1989]. Second, the spectral filtering by the interference filter at the strong emission line at 777.4 nm maximizes the lightning signal relative to the reflected daylight background. Third, the OTD implements a temporal filtering scheme that takes advantage of the difference in lightning pulse duration versus the background illumination seen by each CCD pixel, since the lightning signal-to-noise ratio improves as the integration period approaches the pulse duration. Although an integration time of approximately 1 ms is most appropriate to minimize pulse splitting [*Christian and Goodman*, 1987] and maximize lightning detectability, technological limitations required that a 2 ms integration time be used in the OTD instrument design.

[10] Even with the three "filtering" approaches discussed above, the ratio of the background illumination to the lightning signal can still exceed 100 to 1 at the focal plane. Therefore, a fourth technique, a modified frame-to-frame background subtraction, is implemented to remove the slowly varying background signal from the raw data coming off the OTD focal plane. The real-time data processor generates a precise measurement of the background scene imaged at each pixel of the focal plane array. This back-

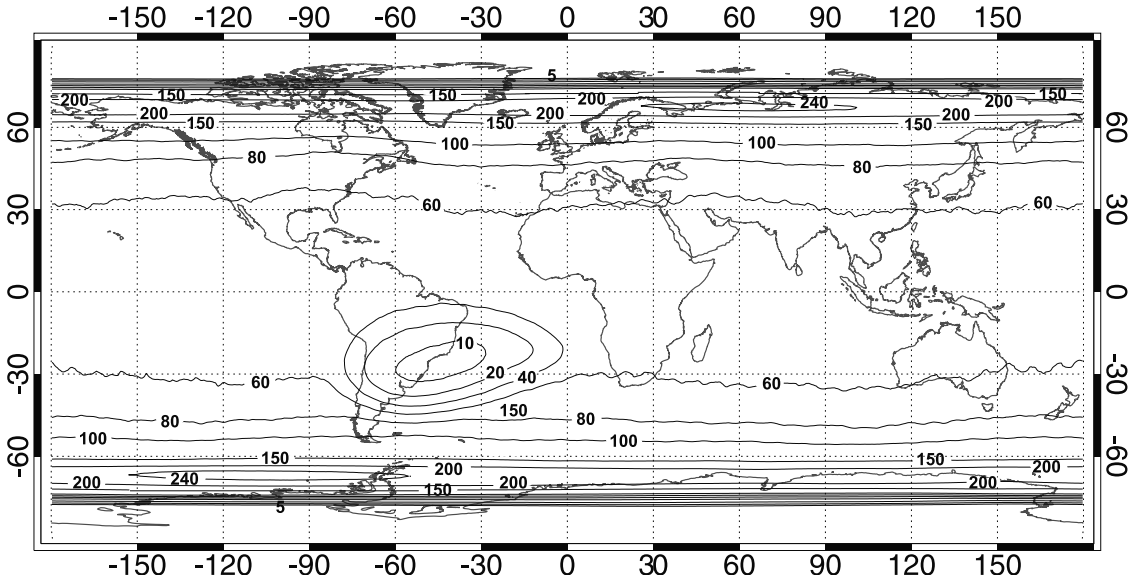

Figure 1. The net amount of time (in hours) that locations on the Earth were within the field of view of the OTD instrument (while operating nominally) during the 5 year period of this study.

ground scene is updated during each frame readout sequence and, at the same time, the background signal is compared with the off-the-focal-plane signal on a pixel-by-pixel basis. When the difference between these signals exceeds a selected threshold, the signal is identified as a candidate lightning "event." The implementation of this Real-Time Event Processor (RTEP) results in a reduction in data rate requirements of greater than a factor of 10^5 while maintaining high detection efficiency for lightning events. The observed events are tagged with a time and location, formatted, queued, and sent to the spacecraft for later transmission to the ground station. In addition, the RTEP also processes an entire background image about once every minute, which is helpful in verifying the satellite navigation information used in geolocating these events.

[11] The instrument/platform configuration allows the OTD to resolve temporally the optical pulses associated with lightning to within 2 ms, to spatially resolve lightning to 8 km at nadir, maintain a 1.6×10^6 km^2 field of view of the Earth (of which 5% is obscured by the OV-1 gravity gradient boom), detect lightning flashes with high, nearly uniform detection efficiency verified to within a relatively high degree of certainty, and identify and locate lightning flashes with nearly the same detection efficiency during the day and night [*Boccippio et al.*, 2002].

[12] The precessing low Earth orbit and 740 km altitude of the OV-1 satellite dictates the temporal and spatial coverage of the Earth by the OTD instrument. The combination of the orbital inclination and the instrument field of view permits OTD to record lightning activity between 75°N and 75°S latitude. Over a 12 month period, the OTD instrument observes most points on Earth for a total time exceeding 14 hours accumulated from more than 400 individual overpasses, although higher latitudes are generally observed more often than equatorial latitudes. Over its 5 year mission, the median and mean total observation times of ground locations included in this study were 58 and 74 hours, corresponding to a total space–time sampling of 1.3×10^{14} km^2 s^{-1} (Figure 1). Lightning can be observed during all hours of the diurnal cycle due to the precession of the orbit relative to the Sun, although 55 days of observation are required for a complete local resampling of the diurnal cycle. The combination of accuracy, stability, sensitivity and sampling combine to yield a set of lightning observations which is superior in many ways to earlier observations from space.

2.2. Measurements and Methodology

[13] The raw OTD data are a list of CCD pixel firings (events) caused by optical pulses and instrumental, optical and environmental noise. The amplitude, pixel location, and time of occurrence of these events are transmitted from the spacecraft to the ground where they are examined, processed and stored in an intermediate data format. Several software algorithms are used to geolocate the events, remove noise [*Boccippio et al.*, 2002], and organize the remaining events into flashes using a clustering algorithm [*Christian et al.*, 2000]. The filtered data correspond to optical emissions from lightning processes, primarily K-changes, dart leaders and return strokes [*Goodman et al.*, 1988; *Thomas et al.*, 2000].

[14] The algorithm used to cluster the events into flashes produces a result consistent with the concept that a lightning flash produces one or more optical pulses that occur in the same storm cell within a specified time and distance. The algorithm tests each event for its spatial and temporal proximity to other events and determines whether each event should be clustered with other events as part of a multiple event flash or should be categorized as a single event flash [*Christian et al.*, 2000]. Specifically, for multiple events to be considered part of the same flash, they must not have more than a 333 ms time gap between successive time frames of events, and they must not have more than 15 km of separation distance between geolocated, neighboring events. The maximum spatial separation distance of 15 km is derived from the resolution of the sensor, and the

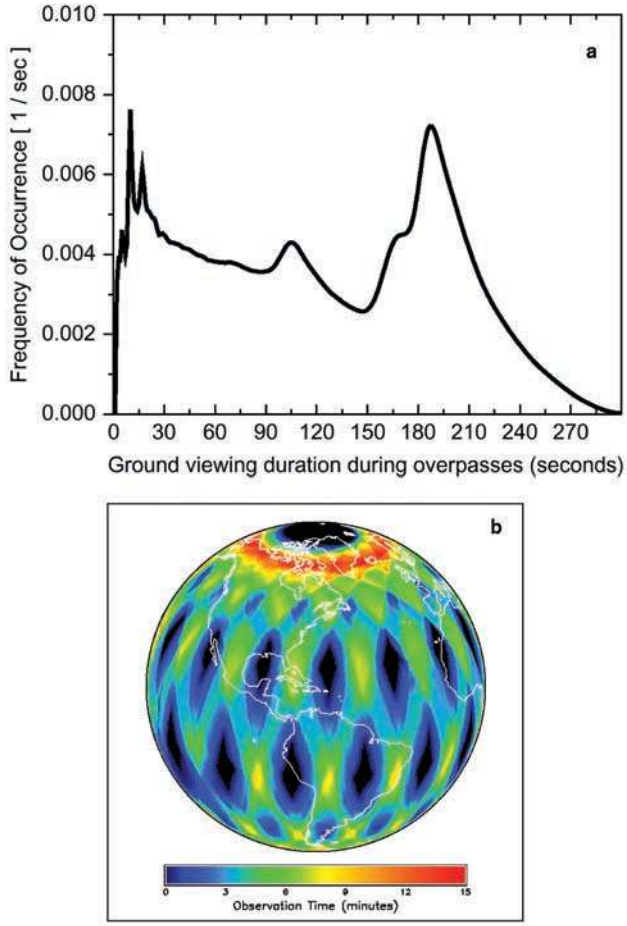

Figure 2. (a) The distribution of viewing durations for 0.5° × 0.5° ground locations during individual OTD overpasses. (b) An example showing the amount of time that various locations on the Earth are within the field of view of the OTD instrument during a 24 hour period.

temporal tolerance of 333 ms arose from a review of prior measurements of lightning activity [*Ogawa*, 1982; *Christian and Goodman*, 1987; *Goodman et al.*, 1988]. Tests of this clustering algorithm showed a good correspondence to the "conventional interpretation" of a flash, although mismatches between algorithm flashes and actual flashes (contiguous channel structures) occasionally occur. Statistical examination of the spectrum of spatiotemporal separation between nominal OTD flashes suggests that the impacts of possible clustering algorithm inaccuracy are small [*Boccippio et al.*, 2000a]. Ambiguity is further mitigated by the fact that instantaneous storm flash rates high enough to yield possible flash overlaps at the OTD pixel resolution (e.g., $\sim$>30 fl min^{-1}) comprise a very small fraction of the overall instantaneous flash rate spectrum [*Williams et al.*, 2000; *Boccippio et al.*, 2000b].

[15] The duration and frequency of the observations made by the OTD instrument is largely dependent upon its orbit and its instantaneous field of view. Since the OTD travels with a velocity of 7 km s^{-1} relative to the surface of the Earth, a position on the Earth can remain within the instrument's field of view for several minutes. The duration of observation depends upon a ground location's distance from the satellite boresight track and the OTD's orientation (primarily yaw), which varies with time (Figure 2a). As demonstrated in Figure 2b, a large percentage of the Earth can be observed at least once by the OTD instrument during a 24 hour period. Due to the inclination of the orbit, locations near the equator are observed less frequently than the higher latitudes, as shown in Figure 1. Additionally, a portion of South America and the adjacent oceans are viewed less frequently, when high radiation levels in the South Atlantic Anomaly [*Pinto et al.*, 1992; *Herlitzer et al.*, 2002] fill the data buffers of the OTD instrument.

[16] When determining the average global flash rate from the OTD data, the number and location of the lightning flashes observed by the OTD instrument were combined with its temporal and spatial coverage of the globe. The surface of the Earth was divided into equal-angle grid cells; 0.5° × 0.5° for an annualized composite, and 2.5° × 2.5° for decomposition of the annual cycle. The number of flashes observed by the OTD and the total viewing time were determined for each grid cell. Flash counts were weighted by the inverse of estimated flash detection efficiency (next section), and flash rates were calculated by dividing the number of flashes detected in a grid cell by the observation time for that cell. The flash rate for the entire globe was calculated as the sum of all grid cell flash rates.

[17] All OTD orbits undergo both automatic and manual quality assurance (QA). In this analysis, any orbits assigned a manual QA warning flag (indicating either actual or potential instrument or spacecraft errors) were rejected. In addition, each OTD flash is assigned an automated quality metric (the "thunderstorm area count" or "density index"), derived from the spatiotemporal frequency of pixel events observed at the flash's ground location. This metric indicates the likelihood that the flash is true lightning rather than optical, instrument or radiation noise [*Christian et al.*, 2000] and is predicated on the observation that the majority of lightning flashes produce many observable optical pulses

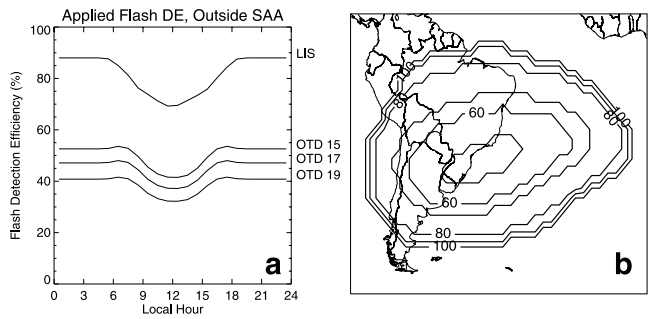

Figure 3. (a) Estimated flash detection efficiencies applied in this analysis, applied as a function of local observation hour for LIS and OTD. Detection efficiency corresponding to OTD thresholds of 15 were applied from 3 May 1995 to 8 June 1995 and 23 October 1996 to 21 March 2001, 17 from 20 July 1995 to 22 October 1996, and 19 from 9 June 1995 to 19 July 1995. (b) Additional multiplicative correction factor for OTD detection efficiencies from (a), correcting for increased activity of radiation noise filters within the South Atlantic Anomaly.

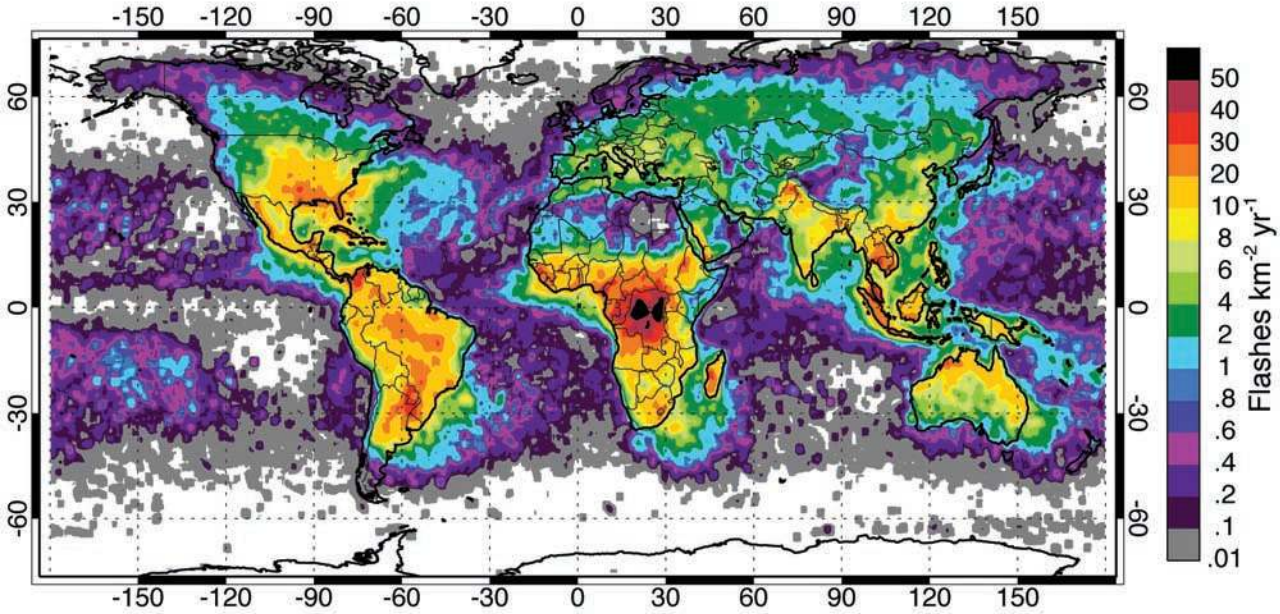

Figure 4. The annualized distribution of total lightning activity (in units of fl km^{-2} yr^{-1}).

[*Goodman et al.*, 1988; *Thomas et al.*, 2000; and unreported analysis of data presented by *Boccippio et al.*, 2001b]. A minimum cutoff value of 140 (arbitrary units) was established for this metric as the most tolerant filter level that removes clearly SAA-related radiation noise; this value is the same used in the validation and science studies of *Boccippio et al.* [2000a, 2000b, 2001a].

[18] Orbital precession of the OTD instrument relative to the Sun was accounted for when determining the flash rate for the globe. Flash rates computed from OTD data will contain a strong diurnal bias if the data are not smoothed over 55 day intervals. A period of 55 days is required for the OTD instrument to observe most locations on the Earth at least once in each (local) hour of the diurnal cycle due to the precession of the satellite's orbit around the Earth's polar axis. Since lightning activity is more frequent during the late afternoon hours, the slow, but constant, orbital precession of the satellite relative to the Sun significantly biases flash rates derived from brief subsets of OTD data. Annual cycles presented in this paper are constructed by summing all

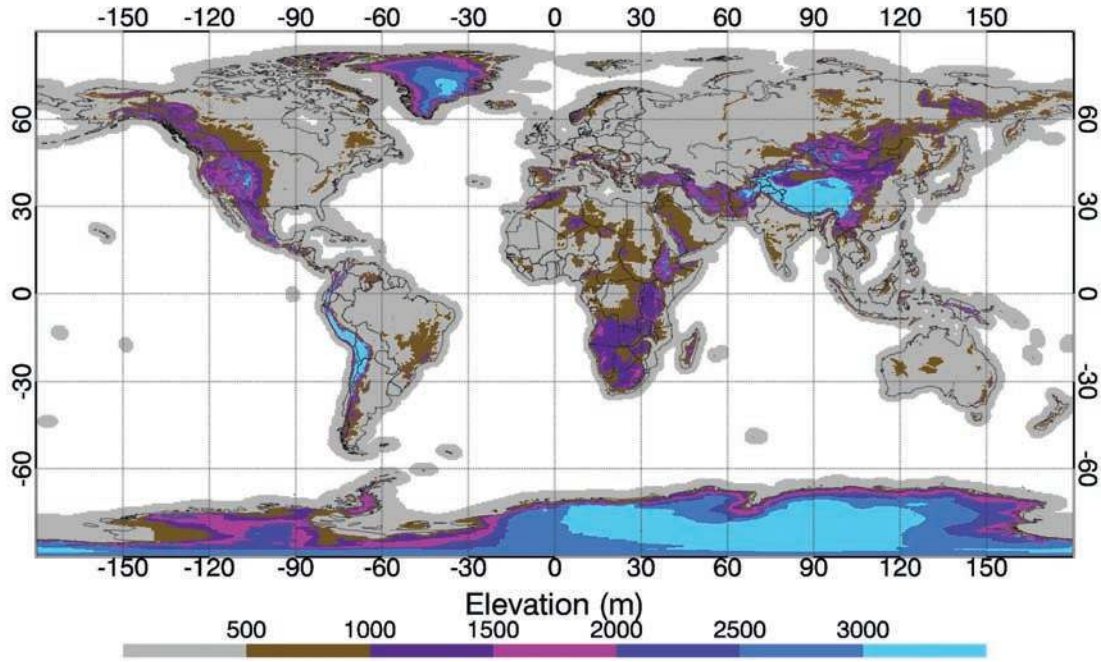

Figure 5. Mask used for land (gray)/ocean (white) and zonal and meridional band definitions, as used in this analysis (Figures 7, 8, and 9). Elevation contoured every 500 m.

Table 1. OTD Mean Annual Flash Density: North America

Rank	Place name	OTD, fl km^{-2} yr^{-1} (CG, fl km^{-2} yr^{-1})	Lat (N)	Lon (E)	Thunder days
1	Tampa–Orlando, FL, US	35.4 (14)	28.75°	−81.75°	91
2	Texarkana, AK, US	33.5 (6)	33.75°	−94.75°	71
3	Palestine, TX, US	33.3 (6)	30.75°	−94.75°	46
4	Mobile, Alabama, US	32.4 (14)	30.75°	−88.75°	64
5	Comalcalco, Mexico	30.8	18.25°	−90.75°	19
6	Manzanillo, Cuba	30.7	20.75°	−77.75°	–
7	Tepic, Mexico	28.7	22.25°	−105.25°	5
8	Arivechi, Mexico	24.0	28.75°	−109.25°	–
9	Abilene, TX, US	23.9 (4)	33.25°	−99.75°	38
10	San Salvador, El Salvador	23.5	13.25°	−88.25°	115
11	Northern Gulf of Mexico	22.9	26.25°	−86.25°	–
12	Gulf Stream-E of Carolinas, US	22.6	32.25°	−77.25°	–
13	Wichita, KS, US	22.3 (4)	37.75°	−98.25°	54
14	Colon, Panama	20.2	9.4°	−79.9°	149

weighted flash counts and viewing times for each day of the year, smoothing these with a 55 day boxcar moving average, and dividing flash counts by viewing times to yield climatological daily flash rates.

2.3. Instrument Sensitivity

[19] The detection efficiency of the OTD instrument is dependent upon the instrument threshold setting, which can be changed by sending a command to the spacecraft. The lowest threshold setting, which corresponds with the highest sensitivity, is an 8-bit value of 14 "digital counts" [*Boccippio et al.*, 2000a]. In order for a flash to be detected by the OTD instrument, at least one of the optical pulses produced during the flash must exceed the detection threshold of the instrument. Each pixel's actual radiance threshold is dependent on the threshold setting, the intensity of the background scene and the instrument response at the observation angle. The number of pulses that are detected during each observed flash is in turn dependent on the actual radiance threshold, the pixel resolution and the amount of light scattered toward the instrument [*Boccippio et al.*, 2002]. For the lower threshold settings, the sensitivity to lightning is high, but these lower thresholds also are susceptible to higher levels of optical, radiation and instrument noise. As a result, there is a trade-off between detection efficiency and false-alarm rate.

[20] In order to quantify the flash detection efficiency of the OTD instrument, both the sensitivity of the instrument and the statistical distribution of the optical pulses produced during lightning discharges were examined. Through detailed measurements made aboard a NASA U-2 aircraft, *Christian and Goodman* [1987] determined that a flash detection efficiency of 90% could be achieved with an optical sensor that can detect a radiant energy density of 4.7 μJ sr^{-1} m^{-2}. For the lowest operating OTD instrument threshold measured during laboratory calibration, *Koshak et al.* [2000a] estimated an average nighttime flash detection efficiency of 76%, based on sampling of pixels in the interior of the CCD array. This estimate has recently been revisited. Using the same approach and accounting for variability in the instrument response across the angular field of view and for the operational threshold of 15 used during most of the mission (23 October 1996 to 21 March 2000), *Boccippio et al.* [2002] estimated the maximum possible nighttime bulk detection as 65%. These authors also predicted a further reduction in detection efficiency based on the statistical likelihood of less light being scattered out of clouds at angles off-normal from cloud top (the U-2 "truth" data set was sampled at angles nearly normal to cloud top, but the OTD cloud observation angle can vary from 0° to 53° across the field of view). Allowing for this correction, the predicted peak nighttime bulk detection efficiency was further lowered to 56%. An approximate 10% reduction was also predicted during daylight hours, as the instrument gain is coupled to the intensity of background scene radiance.

[21] The basis for DE adjustment is the diurnal DE prediction of *Boccippio et al.* [2002], applied at threshold 15 and considering cloud scattering. Three further adjustments are also applied:

1. A ratio of 1.7 is predicted between the detection efficiency of the OTD and of the Lightning Imaging Sensor (LIS), its successor instrument. This ratio is exactly that

Table 2. OTD Mean Annual Flash Density: South America

Rank	Place name	OTD, fl km^{-2} yr^{-1}	Lat (N)	Lon (E)	Thunder days
1	Posadas, Argentina	42.7	−27.75°	−56.25°	57
2	Ocana, Colombia	39.9	8.25°	−74.75°	–
3	Concepcion, Paraguay	37.0	−23.25°	−57.25°	–
4	Campo Grande, Brazil	32.9	−21.25°	−53.75°	97
5	Reconquista, Argentina	32.4	−28.25°	−61.25°	–
6	Porto Nacional, Brazil	31.6	−10.25°	−47.75°	134
7	Belem, Brazil	26.6	−2.25°	−49.75°	80
8	Juiz de Fora, Brazil	25.8	−21.75°	−43.25°	56
9	Maipures, Colombia	24.6	5.25°	−68.25°	–
10	Yurimaguas, Peru	21.6	−4.75°	−75.75°	–
11	Carauari, Brazil	19.6	−4.9°	−66.9°	206

Table 3. OTD Mean Annual Flash Density: Europe

Rank	Place name	OTD, fl km^{-2} yr^{-1}	Lat (N)	Lon (E)	Thunder days
1	Tirana Rinas, Albania	9.4	40.75°	19.75°	–
2	Piacenza, Italy	9.1	44.75°	9.75°	22
3	Naples, Italy	9.0	39.75°	14.75°	15
4	Venezia (Venice), Italy	8.8	45.75°	12.75°	22
5	Sibiu, Romania	8.5	45.75°	23.25°	–
6	Barcelona, Spain	8.1	41.25°	2.25°	30
7	Adana, Turkey	8.0	36.75°	35.25°	27

found in climatological ratios of uncorrected OTD and LIS data [*Boccippio et al.*, 2000b]. The results of *Boccippio et al.* [2002] appear to slightly over predict LIS detection efficiency, based on limited ground validation of that sensor [*Thomas et al.*, 2000; *Koshak et al.*, 2000b]. A 3% downscaling of applied OTD detection efficiency is consistent with both the predicted LIS/OTD ratio and the available empirical estimates of LIS detection efficiency.

2. The diurnal DE curve for threshold 15 is adjusted slightly during periods of different instrument threshold settings (see below); the adjustments derive from the ratios (between threshold settings) of empirically estimated flash detection efficiency reported by *Boccippio et al.* [2000a].

3. The OTD detection efficiency is further reduced during satellite passage through the South Atlantic Anomaly, a high-radiation environment in which adaptive software noise filters must be run more stringently to reject false events. The approximate region impacted by this reduction is roughly the same as that in which viewing is reduced due to instrument data buffer overflows (Figure 3). The impact of this reduction is estimated from the climatological ratio of uncorrected LIS and OTD data in this region (the lower altitude LIS is much less affected by SAA radiation). At the center of the SAA (near Sao Paulo, Brazil), the climatological ratio implies an additional 50% (relative) reduction in OTD detection efficiency. This correction is applied as a spatial adjustment decreasing continuously from no reduction at the SAA periphery to 50% at the SAA core.

[22] The resulting diurnally applied detection efficiencies (for regions outside the SAA) are shown in Figure 3a for the three OTD thresholds used during the mission. The spatial SAA relative correction is shown in Figure 3b. These yield a bulk (mission-averaged) estimate of 49% detection efficiency. Based on empirical comparison of OTD total lightning and National Lightning Detection Network (NLDN) ground strike observations, *Boccippio et al.* [2000a] estimated the OTD cloud-to-ground lightning detection efficiency as 46–70% (for the two thresholds applied during most of the mission, 15 and 17), with a 10% day/night variation. The predicted and empirically estimated detection efficiency are in reasonably good agreement, given that the empirical NLDN study was forced to allow very tolerant spatiotemporal flash matching criteria to compensate for spatial and temporal location errors and differences between OTD optical pulse and NLDN ground stroke times. We estimate the uncertainty in flash DE applied in this study to be ±10%.

3. Results and Discussion

[23] The 5 year OTD average annual and seasonal worldwide distribution of total lightning activity is presented. The global flash rate is further decomposed into its seasonal cycle, and the variation of flash rate is compared between land and ocean, Northern and Southern Hemispheres, tropics and subtropics, and the three major continental landmasses: Africa/Europe, the Americas, and Asia/Maritime Continent.

[24] The global annual average total (intracloud and cloud-to-ground) flash rate is found to be 44 ± 5 fl s^{-1}. The annual global flash rate ranges from a maximum of 55 fl s^{-1} (in Northern Hemisphere summer) to a minimum of 35 fl s^{-1} (in Northern Hemisphere winter). These lightning flash rate estimates are less than half the traditional estimate of 100 fl s^{-1}, proposed by *Brooks* [1925]. Additionally, the OTD derived global flash rate is less than recently published estimates of the average global flash rate, given that these

Table 4. OTD Mean Annual Flash Density: Africa

Rank	Place name	OTD, fl km^{-2} yr^{-1}	Lat (N)	Lon (E)	Thunder days
1	Kamembe, Rwanda	82.7	−1.25°	27.75°	221
2	Boende, Dem. Rep. Congo	66.3	0.25°	20.75°	118
3	Lusambo, Dem. Rep. Congo	52.1	−4.75°	24.25°	119
4	Kananga, Dem. Rep. Congo	50.3	−5.75°	18.75°	139
5	Calabar, Nigeria	47.4	5.25°	9.25°	216
6	Franceville, Gabon	47.1	−2.25°	14.25°	–
7	Miandrivazo, Madagascar	35.9	−19.25°	45.75°	146
8	Mamfe, Camaroon	35.6	5.7°	8.3°	201
9	Kindia, Guinea	35.0	10.75°	−12.75°	111
10	Bahar Dar, Ethiopia	33.1	12.25°	36.75°	–
11	Ouanda Djalle, Central African Republic	31.5	8.25°	22.25°	–
12	Macenta, Guinea	31.4	8.25°	−10.25°	151
13	Jos, Nigeria	29.4	9.25°	8.25°	139
14	Kumasi, Ghana	26.1	6.25°	−1.25°	157
15	Entebbe, Uganda	23.4	0.0°	32.6°	206
16	Sikasso, Mali	23.0	10.75°	−5.75°	123
17	Bloemfontein, South Africa	23.0	−29.75°	28.75°	60

Table 5. OTD Mean Annual Flash Density: Asia

Rank	Place name	OTD, fl km^{-2} yr^{-1}	Lat (N)	Lon (E)	Thunder days
1	Kuala Lumpur, Malaysia	48.3	3.25°	101.75°	180
2	Aranyaprathet, Thailand	36.3	13.75°	102.25°	–
3	Murree, Pakistan	33.3	33.75°	73.25°	72
4	Loc Ninh, Vietnam	32.4	11.75°	106.75°	–
5	Bandung, Indonesia	25.6	−6.25°	106.75°	218
6	Banjarmasin, Indonesia	24.8	−2.75°	114.75°	–
7	Krishnanagar, India	23.0	23.75°	89.25°	108
8	Manila, Philippines	22.4	15.25°	120.25°	60

prior estimates were all greater than 60 fl s^{-1} [*Orville and Spencer*, 1979; *Kotaki and Katoh*, 1983; *Mackerras et al.*, 1998]. Moreover, these prior estimates were reported with a range of uncertainty due to instrument and sampling limitations that approached a factor of two, which is the likely explanation for the discrepancy between the prior estimates and the results obtained from the OTD data. The range of uncertainty associated with the OTD derived global flash rate is estimated to be no more than 20%, a value that primarily reflects uncertainty in the flash detection efficiency of the instrument. The observed OTD flash rate also implies that mean flash dipole moment change is somewhat lower than that used by *Heckman et al.* [1998], assuming that their small sample of SR observations is climatologically representative.

[25] The annual average global distribution of total lightning flash rate is shown in Figure 4. Flash rate is contoured in units of fl km^{-2} yr^{-1}, based on a 0.5° × 0.5° compositing grid smoothed with a 2.5° spatial moving average operator (this resolution is consistent with the navigational uncertainty of the OV-1 platform) [*Boccippio et al.*, 2000a]. The geographical distribution of flash rate density is in general qualitative agreement with the climatological distribution of thunderstorm days [*WMO*, 1953], being dominated by the diurnal heating of the major landmasses. The peak mean annual planetary flash density exceeds 80 fl km^{-2} yr^{-1} and occurs just west of Kamembe, Rwanda, a place that averages 221 thunderstorm days yr^{-1}.

3.1. Flash Rate Extrema

[26] The greatest flash densities occur in coastal areas (e.g., southeastern U.S. coast bordering the Gulf of Mexico and Florida, Panama, Cuba, Bangladesh, Indonesian Archipelago, Naples and Venice, Italy, and Barcelona, Spain) mountainous regions (e.g., Himalayas in northern Pakistan, Sierra Madre of western Mexico, Andes of northern Colombia, Italian Alps), regions frequented by migrating synoptic scale cyclones, and convergence zones such as the South Atlantic Convergence Zone, South Pacific Convergence Zone, and the Intertropical Convergence Zone, which modulates the latitudinal distribution of lightning frequency from the equatorial eastern Pacific through central Africa. Lightning is predominant in the northern Atlantic and western Pacific Ocean basins year-round where instability is produced from cold air passing over warm ocean water. The northern Gulf of Mexico basin and Gulf Stream east of the Carolinas each have a peak flash density in excess of 22 fl km^{-2} yr^{-1}, a value equal to the flash density at Wichita, KS. Lightning is less frequent (and the atmosphere more stable) in the eastern tropical Pacific and Indian Ocean basins where the overlying air mass is warmer.

[27] The equatorial Congo Basin is the "hot spot" of the planet. Within the basin, for example, an area of 3 million km^2 (roughly four times the area of the state of Texas) exceeds the flash rate density of central Florida (30 fl km^{-2} yr^{-1}), the U.S. "hot spot." The sharp maximum flash density gradient along the eastern edge of the Congo Basin is defined by the Mitumba mountain range running N-S along the entire length of the basin. The collective boundaries of the E-W mountain ranges that extend from the European Alps to the Himalayas provide additional orographic foci (flow barriers) for the development of thunderstorms, with a local maximum of 33 fl km^{-2} yr^{-1} in northern Pakistan. The anchoring of thunderstorms tied to the elevated heat sources of cordilleras and other more localized topographic features can be deduced through a comparison between the flash density distribution in Figure 4 and the terrain elevation shown in Figure 5.

[28] Tables 1–6 provide additional detail on the locations having the greatest mean annual flash density within or in close proximity to each of the major continents. A nearby place name in close proximity to the OTD observed maximum and the representative thunder day climatology [*WMO*, 1953] for that same site is also provided, but only if the site is both a reporting station and located in the same or similar climatological regime (i.e., coastal or mountain environment). It should be noted that the WMO thunder day climatology does not contain any station reports for some countries such as Venezuela and Colombia, which encompass the very active northwestern regions of South America; although ground-based lightning measurements in this region indicate there are ∼140 thunder days yr^{-1} (H. Torres, personal communication, 2002).

[29] For the six U.S. stations (Table 1), the mean annual CG flash density (ranging from 4 to 14 fl km^{-2} yr^{-1}) is also shown. The CG flash density is computed from the National Lightning Detection Network (K. Cummins, personal communication, 2002). The tendency toward greater IC/CG ratios of nearly 6:1 in the southern Great Plains (Texarkana, AR; Palestine and Abilene, TX; Wichita, KS) compared with a ratio of ∼2.5:1 at coastal stations (Tampa, FL and Mobile, AL) is consistent with the suggestion that there is a greater predominance of deeper storms and supercells producing more abundant in-cloud lightning extending from the southern through the northern Great Plains states [*Buechler et al.*, 2000; *Boccippio et al.*, 2001a; *McCaul et al.*, 2002].

Table 6. OTD Mean Annual Flash Density: Australia

Rank	Place name	OTD, fl km^{-2} yr^{-1}	Lat (N)	Lon (E)	Thunder days
1	Fitzroy Crossing	33.2	−16.25°	126.25°	–
2	Marble Bar	14.6	−22.25°	117.25°	15
3	Dubbo	13.0	−31.75°	148.75°	14

[30] The flash density maxima do not necessarily coincide with the absolute thunder day maxima, a different index of lightning activity. Indeed, some of the lower flash density maxima ($\sim$20 fl km^{-2} yr^{-1}) correspond to locales having the greatest number of thunder days (e.g., Colon, Panama, Carauari, Brazil, and Entebbe and Kampala, Uganda). We note that a thunder day will give equal contribution to a day having multiple storms, a very active, long-lived convective complex producing thousands of flashes per hour, a supercell storm, or a small isolated thunderstorm. Thus, the flash density embodies both storm intensity and storm frequency. It is also noteworthy that the period 1995–2000 also includes representative climate variations due to both an El Niño (1997–1998) and La Nina (1998–1999) event [*Goodman et al.*, 2000].

[31] The annual average distribution is strongly dependent on the seasonal evolution of regional flash rates. Maps of the seasonal distribution and frequency of lightning activity were computed at 2.5° spatial resolution (Figure 6). Flash density is generally greatest in the respective hemisphere spring and summer seasons over land and year-round in coastal zones.

3.2. The Congo and Amazon Basins

[32] Within the equatorial tropics, there is a large contrast in flash density between the Amazon and Congo basins. The Congo basin has high flash densities year-round, yet there is a shift in maximum flash density northward across the equator between December–February and June–August coupled to the general migration of the Intertropical Convergence Zone (ITCZ) and an associated shift in synoptic scale forcing (wind, pressure, and convergence) and large (>2000 m^2 s^{-2}) Convective Available Potential Energy (CAPE) over equatorial Africa [*Barnes and Newton*, 1982; *Monkam*, 2002]. From December to February the mean vertical ascent is greatest from 0°S to 20°S, bounded on the north by the ITCZ. During the seasonal period June–August the maximum mean vertical ascent shifts northward across the equator extending from 0°N to 20°N [*Ba and Nicholson*, 1998]. The high flash density gradient terminates approximately at the ITCZ, which represents the boundary between two primary air masses; the northernmost extent of the moist westerly air originating in the Atlantic and the dry desert air originating in North Africa. The mountains in east central Africa block the low-level moist easterly flow originating in the Indian Ocean. From $\sim$10°S to 20°S in the south central African countries of Angola and Zambia (including the southern tip of Dem. Rep. Congo) there is a large intraseasonal contrast in lightning activity between the cool, dry season with no lightning at all in June–August and the wet season with a maximum flash density of 30–40 fl km^{-2} yr^{-1} in the period December–February. The largest intraseasonal variations in the tropics are found in northwest Australia near Fitzroy Crossing (Table 6) and in north central Madagascar (Table 4), where the flash density ranges from zero in June–August to 65 and 78 fl km^{-2} yr^{-1}, respectively, in December–February.

[33] The Amazon basin has its greatest flash densities during the transitional months of September–November. This is a period when synoptic scale frontal systems make their way northward into the basin and the storms are more strongly forced, leading to deeper storms with stronger vertical velocities and a more developed mixed phase region with abundant ice particle concentrations [*Boccippio et al.*, 2000b; *Petersen and Rutledge*, 2001]. *Petersen et al.* [2002] cite various factors that modulate the lightning activity, but low-level easterly wind flow (and associated frontal intrusion into the Amazon basin) is determined to be the most important factor (easterly regimes have the higher flash counts). They note that other recent studies of Amazonian storms and their environment have identified accompanying decreases in cloud condensation nuclei (CCN) concentration and CAPE during the lower flash count westerly regimes. The easterly and westerly regimes and associated vertical structure of storms and related lightning activity are associated with the monsoon/break convective regimes identified by *Rutledge et al.* [1992] and *Williams et al.* [1992].

[34] *McCollum et al.* [2000] identified a number of contrasts between equatorial Africa and the Amazon, any of which may contribute to the observed differences in lightning activity. Central African clouds have on average $\sim$50% smaller cloud droplet radii (determined by AVHRR 3.7 μm satellite radiances), more abundant continental CCN (perhaps originating in the Sahel), fewer of the larger maritime CCN (blocked by mountains from their origin in the Indian Ocean), lower total column water vapor (1 cm less than in the Amazon since there is no barrier to the deep layer moisture flux from the western Atlantic into the Amazon Basin), less precipitable water ($\sim$10 mm less than in the Amazon), drier subcloud air, higher cloud bases, and greater topographic relief (Figure 5). It should also be noted that central Africa "stands out" in observations of convective and lightning parameters from a number of recent satellite studies. *Mohr et al.* [1999] found that the distribution of Congo basin minimum MCS 85 GHz brightness temperatures (an indicator of cloud and precipitation ice) was the coldest among several tropical continental regions. *Boccippio et al.* [2000b] found that the Congo exhibited the highest mean cell flash rates of any high-precipitation tropical region/season, as well as highest flashing cell density during thunderstorm outbreaks. They also found the Congo basin to exhibit near-smallest flash optical radiance, and near-smallest flash optical footprint, perhaps both related to unusually high cloud and precipitation ice, and their effects on optical scattering. S. Nesbitt and E. Zipser (personal communication, 2002) find that central Africa has the highest amplitude diurnal cycle in the occurrence of precipitation features with ice-scattering microwave brightness temperature signatures. The Congo basin thus leads annual production not only because of its high annual "duty cycle" (continual thunderstorm occurrence), but also because of a unique local convective spectrum.

3.3. Oceanic Lightning

[35] From the global and seasonal distributions it is apparent that continentality plays an important role in the distribution of lightning, since a large percentage of the global lightning activity occurs over the landmasses [*Landsberg*, 1960; *Court and Griffiths*, 1982]. In an effort to quantify this percentage, the globe was divided into separate

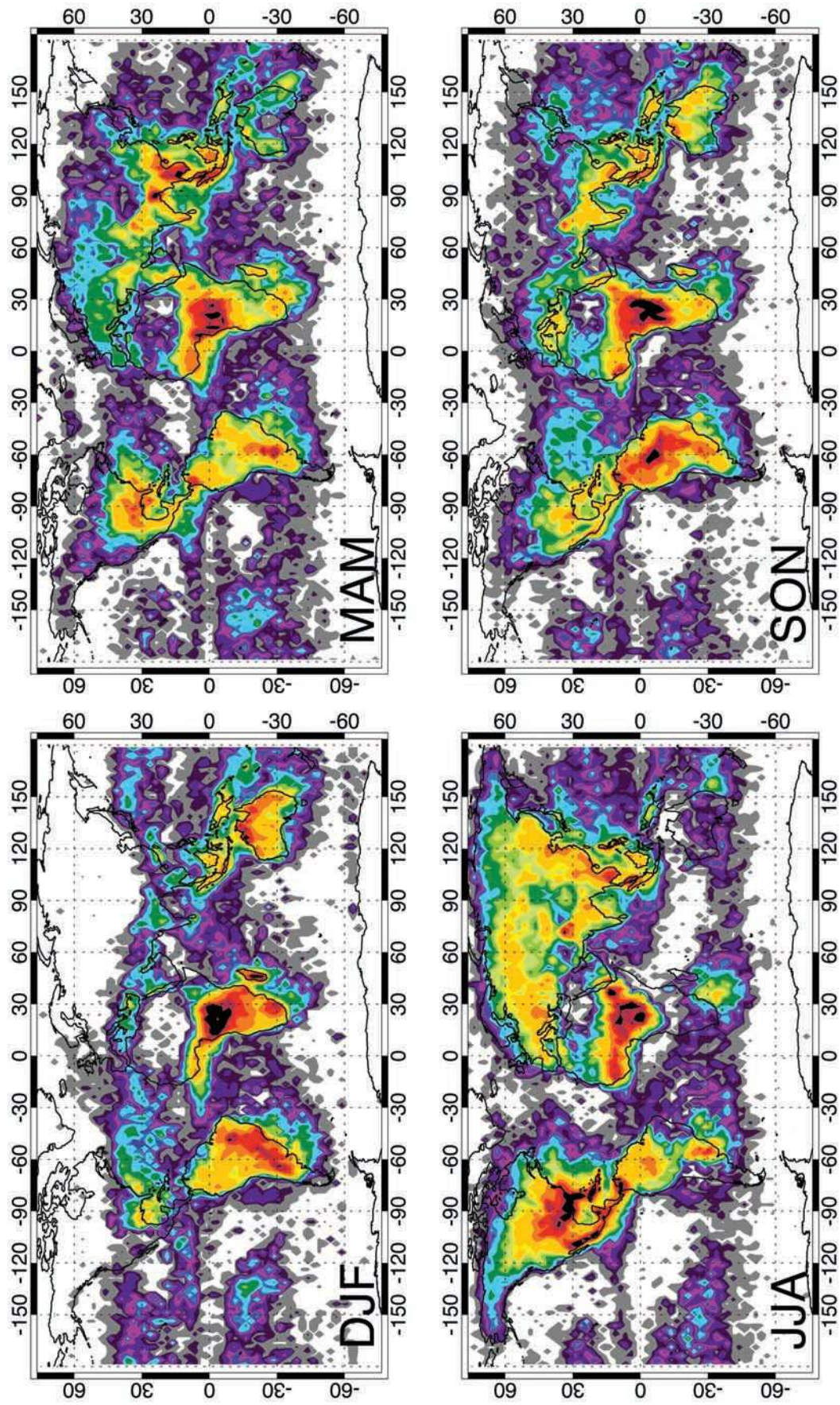

Figure 6. The seasonal distribution of lightning activity (annualized in units of fl km^{-2} yr^{-1}). The contour levels are identical to those of Figure 5. (a) December, January, and February. (b) March, April, and May. (c) June, July, and August. (d) September, October, and November.

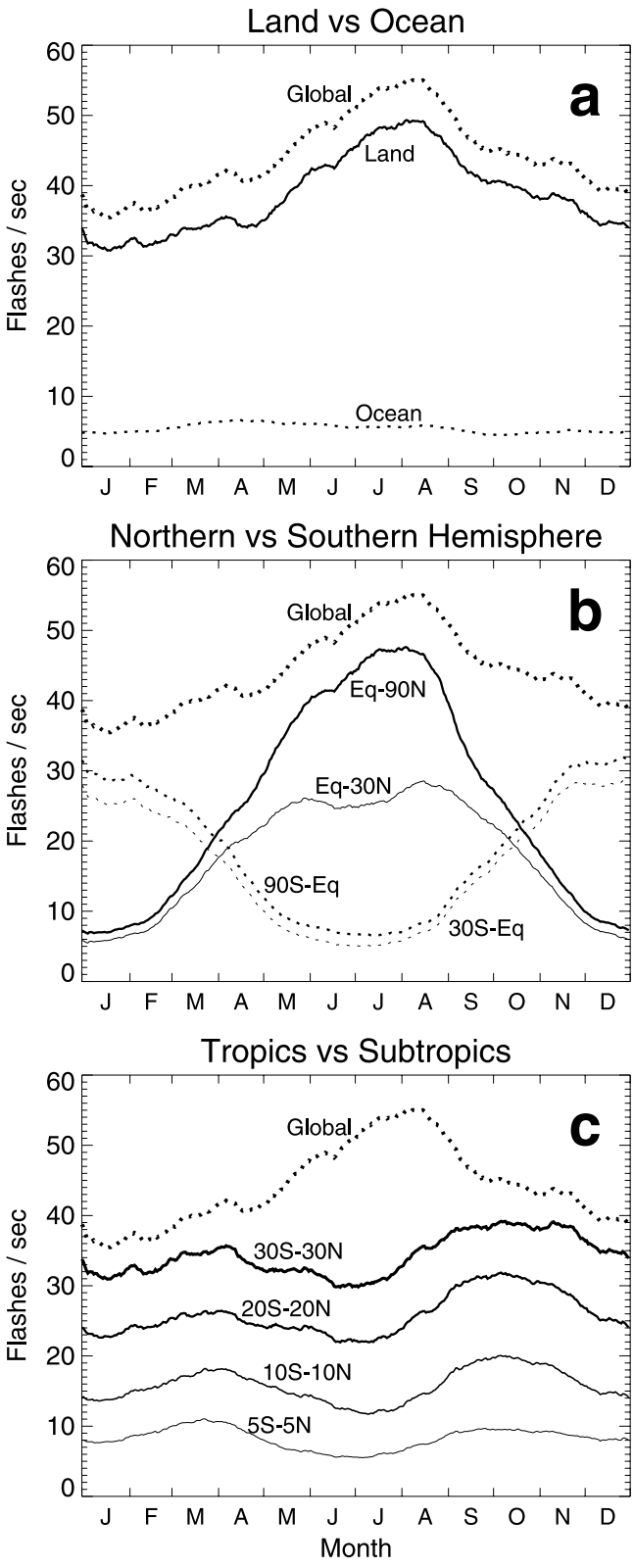

Figure 7. The annual cycle of global flash rate calculated with a 55 day moving average and decomposed into (a) land and ocean contributions, (b) Northern and Southern Hemisphere contributions, and (c) tropical and increasingly subtropical contributions.

land and ocean components, and the annual flash rate was recomputed for both the continental regions and the oceanic regions. The ocean domain (Figure 6) is defined as all 2.5° grid locations with no land cover; the land domain contains all other grid cells (thus the results are additive). The results (Figure 7a), demonstrate that oceanic lightning activity remains fairly constant during the entire 12 month period of observation. The mean annual land to ocean flash ratio is 10:1. The average *global* annual flash rate for the oceanic regions was found to be 5 fl s^{-1}, while continental regions ranged from 31 to 49 fl s^{-1} during the year. Although offshore regions will contain a mix of maritime and migrating continental storms, varying the land mask to a distance of 500 km produced a negligible change in the global land–ocean flash ratio.

[36] The warm waters of the Gulf Stream provide significant boundary layer heat flux and favorable conditions for convection. Enhanced baroclinicity and vertical motion, which in turn will produce more persistent and widespread lightning activity, occurs in association with synoptic scale southwesterly flow ahead of frontal passages and upper-level troughs [*Dirks et al.*, 1988]. Cyclogenesis and frontal passages are responsible for much of the wintertime thunderstorm activity over the Gulf Stream near the east coast of the United States and in the northern Gulf of Mexico [*Goodman et al.*, 2000], both being coastal–oceanic regions of high flash density (Table 1). A similar seasonal variation occurs in the Mediterranean Sea with peak activity in its western and central basin during September–November and in the eastern basin during December–February. The South Pacific Convergence Zone is a region of enhanced oceanic thunderstorm activity year-round, but the central North Pacific Basin is most active in the period from late Autumn through Winter when eastward propagating frontal systems are more common. In the Southern Hemisphere the land–sea temperature contrast and semipermanent high pressure centers in the southern Atlantic and Indian oceans, and Australia are major factors in producing year-round thunderstorm activity extending eastward from the southeast coasts of South America, Africa, and Australia for thousands of kilometers [*Barnes and Newton*, 1982].

3.4. Zonal and Meridional Contributions

[37] By dividing the globe into latitudinal sections, a better understanding of the annual variation in the global flash rate can be obtained. For example, by separately computing the flash rate for the Northern and Southern Hemispheres, it is apparent that the maximum flash rates for each hemisphere occur approximately 6 months apart and occurs during the corresponding summer season, as shown in Figure 7b. The maximum flash rate for the Northern Hemisphere, however, is significantly greater than the maximum flash rate for the Southern Hemisphere. Effectively, lightning activity in North America and northern Asia is responsible for an imbalance in the annual cycle of the global flash rate during the summer months of the Northern Hemisphere.

[38] By dividing the globe into latitude bands, the contribution of the tropics to the global flash rate becomes apparent. As shown in Figure 7c, the frequency of lightning activity for the globe was subdivided into zones consisting

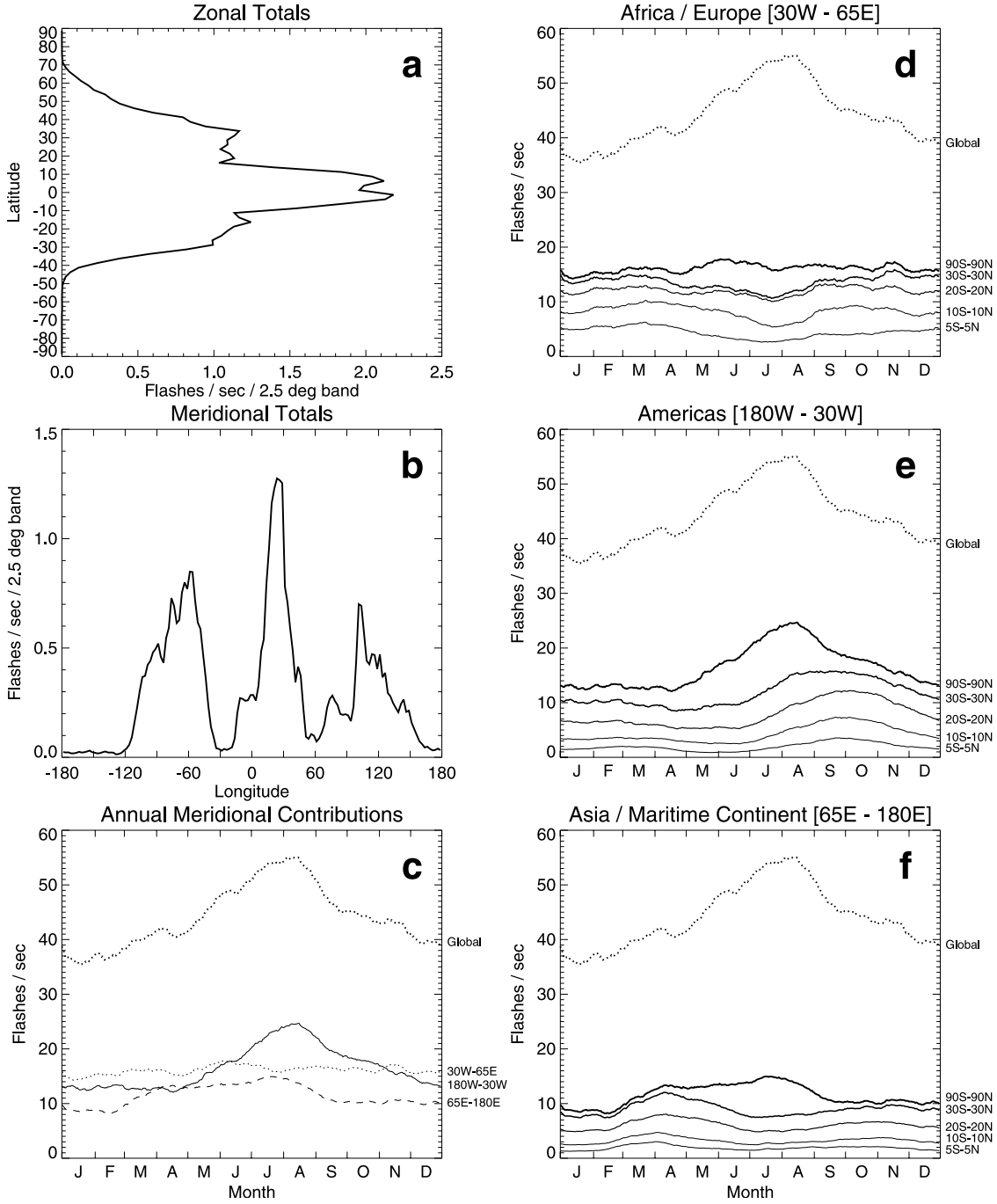

Figure 8. The annual cycle of global flash rate decomposed zonally and meridionally. (a) Zonal total flash rate in 2.5° latitude bands. (b) Meridional total flash rate in 2.5° longitude bands. (c) Meridional contributions corresponding roughly to the Americas, Europe and Africa, and Asia and the Maritime Continent. (d–f) Annual cycles for the three main land regions decomposed into their tropical and subtropical components.

of 5°S to 5°N latitude, 10°S to 10°N latitude, 20°S to 20°N latitude, and 30°S to 30°N latitude Some evidence of a semiannual cycle is found, peaking, as expected, near the equinoxes, with the autumnal equinox dominating. Evidence of a semiannual signal in both fractional deep cloudiness and lightning activity has also been reported by *Williams* [1994], *Kent et al.* [1995], *Satori and Zeiger* [1996], and *Fullekrug and Fraser-Smith* [1997]. Although 78% of global lightning production occurs in the 30°S–30°N band, the evolution of the global annual cycle is nonetheless dominated by the Northern Hemisphere extratropical summer.

[39] Figures 8a and 8b present zonal and meridional totals of annual average flash rate in 2.5° bands. From Figure 8a, it is clear that the tropical bands from roughly 10°S to 10°N contribute nearly twice as much to global

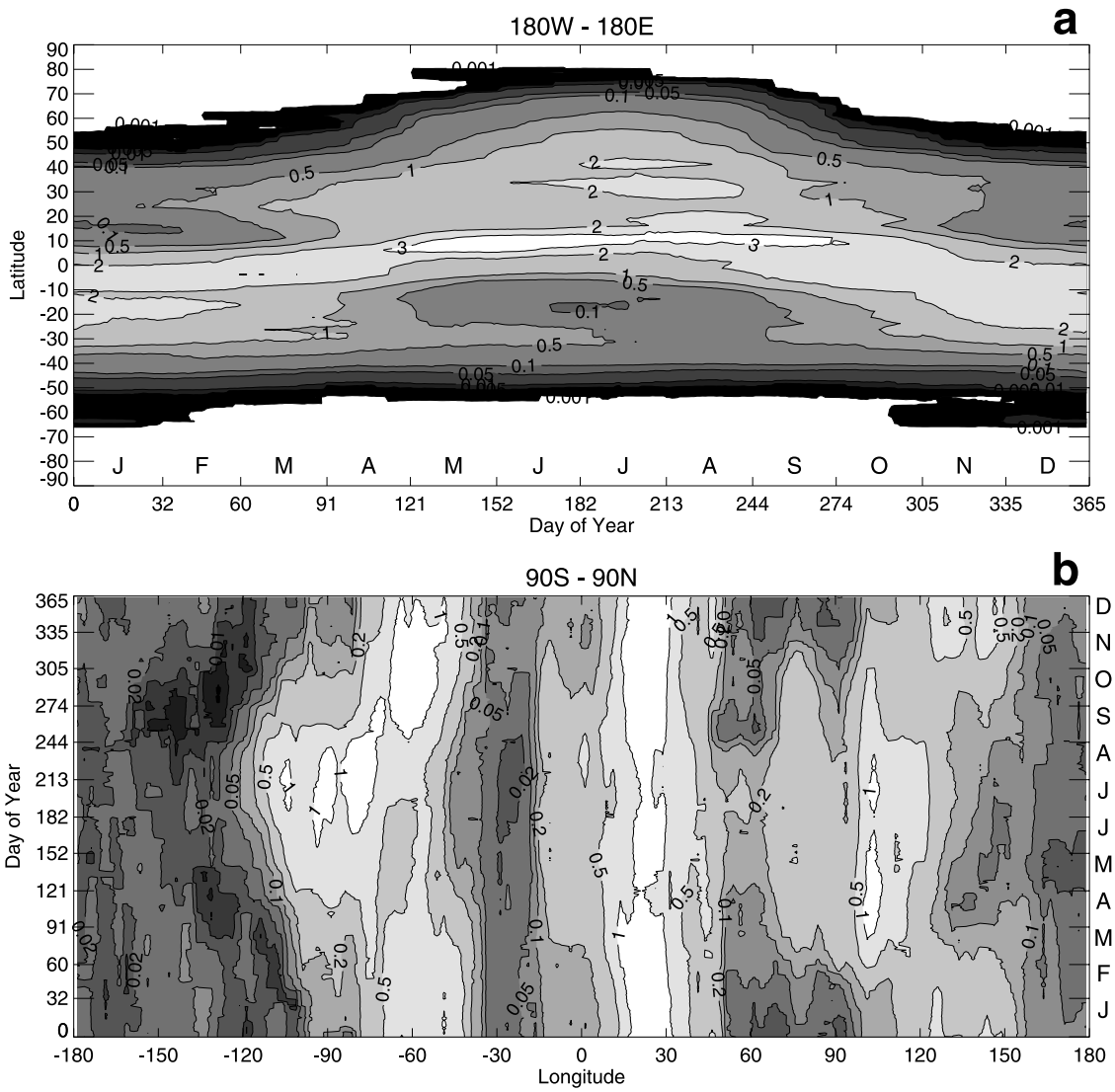

Figure 9. Zonal and meridional band annual cycles of total flash rate (units of fl s^{-1} per 2.5° band).

lightning production as subtropical bands (this can also be inferred from Figure 7c). Given the dominance of land distribution effects on the global distribution, the bimodal peak around the equator likely does not indicate evidence of a split Intertropical Convergence Zone (ITCZ) in global lightning. While the meridional distribution in Figure 8b reveals a sharp local peak in Africa, separation into contributions from the Americas (180°–30°W), Europe and Africa (30°W–65°E) and Asia and the Maritime Continent (65°–180°E) (Figure 8c) suggests that the net contributions from the Americas and Europe/Africa are roughly comparable, at least within these meridional bounds. The meridional contribution of the continents to the mean annual flash density, led by Africa and followed by the Americas and Asia, agrees with that of *Brooks* [1925].

[40] Figures 8d–8f reveal that the apparent global tropical and subtropical semiannual signal (Figure 7c) receives unequal contributions from the three primary land zones. South America dominates the autumnal peak, while South and Southeast Asia contribute strongly to the vernal peak. The African semiannual signal is more symmetric. Extratropical North America clearly dominates the global annual cycle. Figures 9a and 9b further decompose the annual cycle, revealing expected seasonal shifts in the bands of peak lightning production and further illustrating the hemispheric asymmetry. The local minima in Figure 9b additionally help justify the meridional boundaries selected in Figures 8c and 8f.

4. Conclusions

[41] Data from the OTD have been used to determine the average global flash rate, the annual variation of the global flash rate, and the seasonal distribution of lightning. A thorough analysis of the data suggests that the annual average global flash rate, which includes both intracloud and cloud-to-ground lightning, is 44 fl s^{-1}, with an estimated uncertainty that does not exceed ±5 fl s^{-1}. The range of uncertainty *for these global totals* is primarily attributable to uncertainty (and variability) in the flash detection efficiency of the instrument. For other applications (e.g., comparisons of spatially local, diurnal or

interannual variability), uncertainty due to undersampling may dominate.

[42] It is important to note that significantly higher uncertainty, or lower detection efficiency, than we assume is *not* supported either by aircraft observations and instrument sensitivity modeling [*Goodman et al.*, 1988; *Koshak et al.*, 2000a; *Boccippio et al.*, 2002], ground validation of the OTD [*Boccippio et al.*, 2000a], or ground validation of the LIS and cross comparison of the OTD and LIS data [*Thomas et al.*, 2000; *Boccippio et al.*, 2000b; *Koshak et al.*, 2000b]. Given the uncertainty and implicit biases in prior global flash rate estimates, we conclude that the inferred 44 ± 5 fl s^{-1} estimate is the most accurate to date.

[43] Approximately 78% of all lightning occurs between 30°S and 30°N latitudes, and while the annual variation of tropical flash rate is fairly small (of order 10%), there appears to be some evidence of a semiannual modulation. The global annual cycle is dominated by land contributions in the Northern Hemisphere summer, and peaks more than a month after the Northern Hemisphere summer solstice. Continental, island and coastal regions contribute 88% of the global total production. Evidence of a tropical and subtropical semiannual cycle is also found. South and Southeast Asia and equatorial Africa dominate the vernal maximum, while equatorial–subtropical Africa and South America dominate the autumnal maximum. Africa exhibits less semiannual asymmetry than either South America or Southeast Asia.

[44] **Acknowledgments.** Data used in this study were taken from the v0.1 LIS/OTD gridded climatologies, available for order from the Global Hydrology Resource Center (http://ghrc.msfc.nasa.gov). The LIS/OTD instrument team was funded by the NASA Earth Science Enterprise (ESE) Earth Observing System (EOS) project. Additional validation activities were supported by NRA 97-MTPE-03 under the direction of David O'C. Starr.

References

Ba, M. B., and S. E. Nicholson, Analysis of convective activity and its relationship to the rainfall over the Rift Valley Lakes of east Africa during 1983–90 using the Meteosat infrared channel, *J. Appl. Meteorol.*, *37*, 1250–1264, 1998.

Barnes, S. L., and C. W. Newton, Thunderstorms in the synoptic setting, in *Thunderstorms: A Social, Scientific, and Technological Documentary, Vol. 2, Thunderstorm Morphology and Dynamics*, edited by E. Kessler, pp. 109–171, U.S. Dept. of Commer., Washington, D. C., 1982.

Boccippio, D. J., K. T. Driscoll, W. J. Koshak, R. J. Blakeslee, W. L. Boeck, D. A. Mach, D. E. Buechler, H. J. Christian, and S. J. Goodman, The Optical Transient Detector (OTD): Instrument characteristics and cross-sensor validation, *J. Atmos. Oceanic Technol.*, *17*, 441–458, 2000a.

Boccippio, D. J., S. J. Goodman, and S. Heckman, Regional differences in tropical lightning distributions, *J. Appl. Meteorol.*, *39*, 2231–2248, 2000b.

Boccippio, D. J., K. L. Cummins, H. J. Christian, and S. J. Goodman, Combined satellite and surface-based estimation of the intracloud:-cloud-to-ground lightning ratio over the continental United States, *Mon. Weather Rev.*, *129*, 108–122, 2001a.

Boccippio, D. J., S. Heckman, and S. J. Goodman, A diagnostic analysis of the Kennedy Space Center LDAR network, 2, Cross-sensor studies, *J. Geophys. Res.*, *106*, 4787–4796, 2001b.

Boccippio, D. J., W. J. Koshak, and R. J. Blakeslee, Performance assessment of the Optical Transient Detector and Lightning Imaging Sensor, I, Predicted diurnal variability, *J. Atmos. Oceanic Technol.*, *19*, 1318–1332, 2002.

Brooks, C. E. P., The distribution of thunderstorms over the globe, *Geophys. Memo.*, *3*(24), 147–164, 1925.

Buechler, D. E., K. T. Driscoll, S. J. Goodman, and H. J. Christian, Lightning activity within a tornadic thunderstorm observed by the Optical Transient Detector (OTD), *Geophys. Res. Lett.*, *27*, 2253–2256, 2000.

Christian, H. J., and S. J. Goodman, Optical observations of lightning from a high altitude airplane, *J. Atmos. Oceanic Technol.*, *44*, 701, 1987.

Christian, H. J., R. J. Blakeslee, and S. J. Goodman, The detection of lightning from geostationary orbit, *J. Geophys. Res.*, *94*, 13,329–13,337, 1989.

Christian, H. J., R. J. Blakeslee, S. J. Goodman, and D. M. Mach (Eds.), *Algorithm Theoretical Basis Document* (*ATBD*) *for the Lightning Imaging Sensor* (*LIS*), 53 pp., NASA/Marshall Space Flight Cent., Alabama, 2000. (Available as http://eospso.gsfc.nasa.gov/atbd/listables.html, posted 1 Feb. 2000)

Court, A., and J. F. Griffiths, Thunderstorm climatology, in *Thunderstorms: A Social, Scientific, and Technological Documentary, Vol. 2, Thunderstorm Morphology and Dynamics*, edited by E. Kessler, pp. 11–52, U.S. Dept. of Commer., Washington, D. C., 1982.

Dirks, R. A., J. P. Kuettner, and J. A. Moore, Genesis of Atlantic Lows Experiment (GALE): An overview, *Bull. Am. Meteorol. Soc.*, *69*, 148–160, 1988.

Fullekrug, M., and A. C. Fraser-Smith, Global lightning and climate variability inferred from ELF magnetic field variations, *Geophys. Res. Lett.*, *24*, 2411–2414, 1997.

Goodman, S. J., H. J. Christian, and W. D. Rust, A comparison of the optical pulse characteristics of intracloud and cloud-to-ground lightning as observed above clouds, *J. Appl. Meteorol.*, *27*, 1369–1381, 1988.

Goodman, S. J., and H. J. Christian, Jr., Global observations of lightning, in *Atlas of Satellite Observations Related to Global Change*, edited by R. J. Gurney et al., pp. 191–219, Cambridge Univ. Press, Cambridge, 1993.

Goodman, S. J., D. E. Buechler, K. Knupp, K. T. Driscoll, and E. W. McCaul, The 1997–1998 El Niño event and related wintertime lightning variations in the Southeastern United States, *Geophys. Res. Lett.*, *27*, 541–544, 2000.

Hamid, E. F., Z.-I. Kawasaki, and R. Mardiana, Impact of the 1997–98 El Niño event on lightning activity over Indonesia, *Geophys. Res. Lett.*, *28*, 147–150, 2001.

Heckman, S. J., E. Williams, and B. Boldi, Total global lighting inferred from Schumann resonance measurement, *J. Geophys. Res.*, *103*, 31,775–31,779, 1998.

Herlitzer, J. R., J. H. Allen, and D. C. Wilkinson, Ever-present South Atlantic Anomaly damages spacecraft, *Eos*, *83*(15), 165–169, 2002.

Kent, G. S., E. R. Williams, P.-H. Wang, M. P. McCormick, and K. M. Skeens, Surface temperature related variations in tropical cirrus cloud as measured by SAGE II, *J. Clim.*, *8*, 2577–2594, 1995.

Koshak, W. J., J. W. Bergstrom, M. F. Stewart, H. J. Christian, J. M. Hall, and R. J. Solakiewicz, Laboratory calibration of the Optical Transient Detector and Lightning Imaging Sensor, *J. Atmos. Oceanic Technol.*, *17*, 905–915, 2000a.

Koshak, W. J., E. P. Krider, and D. J. Boccippio, LIS validation at the KSC-ER, *Eos*, *81*(48), F47, 2000b.

Kotaki, M., and C. Katoh, The global distribution of thunderstorm activity observed by the Ionospheric Sounding Satellite (ISS-b), *J. Atmos. Terr. Phys.*, *45*, 843–847, 1983.

Landsberg, H., *Physical Climatology*, 2nd edition, Gray Printing Co., DuBois, Pa., 1960.

Levy, H., II, W. J. Moxim, and P. S. Kasibhatla, A global three-dimensional time-dependent lightning source of tropospheric NOx, *J. Geophys. Res.*, *101*, 22,911–22,922, 1996.

Mackerras, D., M. Darveniza, R. E. Orville, E. R. Williams, and S. J. Goodman, Global lightning total, cloud and ground flash estimates, *J. Geophys. Res.*, *103*, 19,791–19,809, 1998.

McCaul, E. W., D. E. Buechler, S. Hodanish, and S. J. Goodman, The Almena, Kansas tornadic storm of 3 June 1999: A long-lived supercell with very little cloud-to-ground lightning, *Mon. Weather Rev.*, *130*, 407–415, 2002.

McCollum, J. R., A. Gruber, and M. B. Ba, Discrepancy between gauges and satellite estimates of rainfall in equatorial Africa, *J. Appl. Meteorol.*, *39*, 666–679, 2000.

Mohr, K. I., J. S. Famiglietti, and E. J. Zipser, The contribution to tropical rainfall with respect to convective system type, size and intensity estimated from 85-GHz ice-scattering signature, *J. Appl. Meteorol.*, *38*, 596–606, 1999.

Monkam, D., Convective available potential energy (CAPE) in northern Africa and tropical Atlantic and study of its connections with rainfall in Central an west Africa during summer 1985, *Atmos. Res.*, *62*, 125–147, 2002.

Ogawa, T., The lightning current, in *CRC Handbook of Atmospherics*, edited by H. Volland, pp. 23–63, CRC Press, Boca Raton, Fla., 1982.

Orville, R. E., and R. Henderson, Global distribution of midnight lightning: September 1977 to August 1978, *Mon. Weather Rev.*, *114*, 2640, 1986.

Orville, R. E., and R. W. Henderson, Absolute spectral irradiance measurements of lightning from 375 to 880 nm, *J. Atmos. Sci.*, *41*, 3180–3187, 1984.

Orville, R. E., and D. W. Spencer, Global lightning flash frequency, *Mon. Weather Rev.*, *107*, 934–943, 1979.

Petersen, W. A., and S. A. Rutledge, Regional variability in tropical convection: Observations from TRMM, *J. Clim.*, *14*, 3566–3586, 2001.

Petersen, W. A., S. W. Nesbitt, R. J. Blakeslee, R. Cifelli, P. Hein, and S. A. Rutledge, TRMM observations of intraseasonal variability in convective regimes over the Amazon, *J. Clim.*, *15*, 1278–1294, 2002.

Pinto, O., Jr., W. D. Gonzalez, I. R. C. A. Pinto, A. L. C. Gonzalez, and O. Mendes Jr., The South Atlantic Magnetic Anomaly: Three decades of research, *J. Atmos. Terr. Phys.*, *54*, 1129–1134, 1992.

Rutledge, S. A., E. R. Williams, and T. D. Keenan, The Down Under Doppler and Electricity Experiment (DUNDEE): Overview and preliminary results, *Bull. Am. Meteorol. Soc.*, *73*, 3–16, 1992.

Satori, G., and B. Zeiger, Spectral characteristics of Schumann resonances observed in central Europe, *J. Geophys. Res.*, *101*, 29,669, 1996.

Thomas, R. J., P. R. Krehbiel, W. Rison, T. Hamlin, D. J. Boccippio, S. J. Goodman, and H. J. Christian, Comparison of ground-based 3-dimensional lightning mapping observations with satellite-based LIS observations in Oklahoma, *Geophys. Res. Lett.*, *27*, 1703–1706, 2000.

Williams, E. R., The Schumann Resonance: A global tropical thermometer, *Science*, *256*, 1184–1187, 22 May 1992.

Williams, E. R., Global circuit response to seasonal variations in global surface air temperature, *Mon. Weather Rev.*, *122*, 1917, 1994.

Williams, E. R., and S. J. Heckman, The local diurnal variation of cloud electrification and the global diurnal variation of negative charge on earth, *J. Geophys. Res.*, *98*, 5221–5234, 1993.

Williams, E. R., S. A. Rutledge, S. C. Geotis, N. Renno, E. Rasmussen, and T. Rickenbach, A radar and electrical study of tropical hot towers, *J. Atmos. Sci.*, *49*, 1386–1395, 1992.

Williams, E., K. Rothkin, D. Stevenson, and D. Boccippio, Global lightning variations caused by changes in thunderstorm flash rate and by changes in the number of thunderstorms, *J. Appl. Meteorol.*, *39*, 2223–2230, 2000.

World Meteorological Organization (WMO), World distribution of thunderstorm days, Publ. 21, TP 6 and Suppl. (1956), WMO, Geneva, Switzerland, 1953.

R. J. Blakeslee, D. J. Boccippio, H. J. Christian, S. J. Goodman, and W. J. Koshak, NASA Marshall Space Flight Center, Huntsville, AL 35805, USA.

W. L. Boeck, Niagara University, Niagara, NY 14109, USA.

D. E. Buechler, K. T. Driscoll, D. M. Mach, and M. F. Stewart, University of Alabama in Huntsville (UAH), Huntsville, AL 35805, USA.

J. M. Hall, CSC Huntsville, Huntsville, AL 35805, USA.